universe

MDPI

Article

Chaos in a Magnetized Brane-World Spacetime Using Explicit Symplectic Integrators

Airong Hu [1,2] and Guoqing Huang [1,*]

[1] School of Physics and Materials, Nanchang University, Nanchang 330031, China; huairong@ncu.edu.cn
[2] School of Civil Engineering and Architecture, Nanchang University, Nanchang 330031, China
* Correspondence: huanggq@ncu.edu.cn

Abstract: A brane-world metric with an external magnetic field is a modified theory of gravity. It is suitable for the description of compact sources on the brane such as stars and black holes. We design a class of explicit symplectic integrators for this spacetime and use one of the integrators to investigate how variations of the parameters affect the motion of test particles. When the magnetic field does not vanish, the integrability of the system is destroyed. Thus, the onset of chaos can be allowed under some circumstances. Chaos easily occurs when the electromagnetic parameter becomes large enough. Dark matter acts as a gravitational force, so that chaotic motion can become more obvious as dark matter increases. The gravity of the black hole is weakened with an increasing positive cosmological parameter; therefore, the extent of chaos can be also strengthened. The proposed symplectic integrator is applied to a ray-tracing method and the study of such chaotic dynamics will be a possible reference for future studies of brane-world black hole shadows with chaotic patterns of self-similar fractal structures based on the Event Horizon Telescope data for M87* and Sagittarius A*.

Keywords: modified theory of gravity; black holes; magnetic fields; chaos; symplectic integrators

Citation: Hu, A.; Huang, G. Chaos in a Magnetized Brane-World Spacetime Using Explicit Symplectic Integrators. *Universe* **2022**, *8*, 369. https://doi.org/10.3390/universe8070369

Academic Editors: Xue-Mei Deng and Lorenzo Iorio

Received: 28 April 2022
Accepted: 30 June 2022
Published: 4 July 2022

1. Introduction

Black holes are solutions of Einstein's general relativistic field equations. The asymmetric bright emission ring and linear-polarimetric EHT images [1,2] of the supermassive black hole(M87) and the gravitational wave from a binary black hole merger (GW150914) [3] confirmed the prediction of Einstein's theory of general relativity about the existence of black holes.

Although the standard theory of relativity has attained much success, it does not fully satisfy observational needs. Some non-general relativistic black holes are considered to test general relativity and to account for related observational results. That is to say that alternative theories of gravity are necessarily used. Besides brane-world spacetimes [4–6], many other alternative theories of gravity with extra fields have been researched in the literature. Some examples are scalar-tensor theories including the Brans–Dicke theories [7–10] and general scalar-tensor theories [11–16], Einstein–æther theory [17], Bimetric theories [18–20], tensor–vector–scalar theories [21–24], scalar–tensor–vector theories [25,26], and Einstein–Cartan–Sciama–Kibble theories [27,28]. There are models of higher derivative and non-local theories of gravity, such as f(R) theories [29–33], f(G) theories [34–36], Hořava-Lifschitz gravity [37–39], as well as Galileons [40,41]. The other forms of modified theories of gravity with higher dimensions include Kaluza–Klein theories [42–44], the Brane cosmology or higher co-dimension brane-worlds [45–48] and Einstein–Gauss–Bonnet gravity [49]. In fact, not all solutions in modified theories of gravity must necessarily satisfy the Einstein field equations. However, the γ metric (or Zipoy–Voorhees metric) [50,51], which describes a static and axially symmetric field departure from the Schwarzschild spacetime with a real positive deformation parameter $\gamma(\neq 1)$, is an exact solution of Einstein's equations in a vacuum. The Kerr metric also remains a solution of certain f(R) theory [52].

In general relativity, the geodesics of curved spacetimes, such as Schwarzschild [53], Reissner–Nordström [54,55], and Kerr [56] black hole, are highly nonlinear. However, they are integrable because enough conserved quantities of motion are present. When these black holes suffer from some perturbations, such as external magnetic field [57–60] and the discs or rings around black holes [61,62], the spacetimes may be non-integrable. In this case, chaos may occur. In fact, the high nonlinearity of general relativity provides a rich source for the study of chaotic dynamics. In addition, the theory of chaotic dynamics may be useful in explaining some astrophysical mechanisms. For example, Stuchlík and Kološ employed the theory of chaotic scattering to explore charged particle ejection [63]. They found that an energy interchange between one energy mode along the magnetic field lines direction and another energy mode at the perpendicular direction arises due to the chaotic charged particle dynamics in the combined gravitational and magnetic fields. In this manner, sufficient energy is given to ultra-relativistic motions of the charged particle along the magnetic field lines. Chaos may have some astronomical observational effects. For instance, the authors of [64,65] pointed out that the lensing of light around rotating boson stars and Kerr black holes with scalar hair has chaotic patterns, and the black hole shadows exhibit self-similar fractal structures. Because of the importance of the chaotic dynamics, there have been a number of papers [66–69] on the chaotic behavior in relativistic astrophysics. Chaos is also considered in modified theories of gravity. The Ernst–Schwarzschild spacetime is non-integrable and can be chaotic in the case without the inclusion of external magnetic fields [70,71]. The γ metric is not integrable either [72]. Chaos can exist in the deformed Schwarzschild spacetimes with external magnetic fields [73,74].

Such general relative systems are higher nonlinear and usually non-integrable. It is difficult or impossible to write analytical solutions for them. Therefore, numerical integration methods are necessary to study the dynamics of these systems. Runge–Kutta methods are often used. However, the family of Runge–Kutta methods are not suitable for a long-time evolution because various errors quickly accumulate with time. Using Lagrange multipliers, Nacozy [75] added a stabilizing terms to the numerical solutions and made the integral more accurate than the uncorrected solutions. According to this basic idea, several authors extended the application of manifold correction methods. The scaling method of Fukushima [76] and the velocity scaling method of Ma et al. [77] exactly conserved energy. Manifold correction methods in references [78,79] are efficient for compensating the defect of Runge–Kutta methods. By taking the slowly varying individual Kepler integrals as integral invariant relations, Deng et al. [80] applied the Kepler analytical solver of the two-body problem to N-body simulations and achieved the best performance. However, such correction schemes do not guarantee the preservation of structural properties.

There are a class of energy-preserving methods that can exactly preserve the energies via a suitable discretization-averaging of the Hamiltonian gradient [81]. Several energy-conserving integrators are designed for conservative Hamiltonian systems of black holes and spinning compact binaries [82–84]. The energy-preserving methods are implicitly non-symplectic.

For a long-term integration, symplectic methods are prior to other non-symplectic algorithms. Symplectic methods share the conservation properties, which include structures, integrals, symmetries, phase space volumes, etc. When a Hamiltonian system is separated into two integrable parts with analytical solutions as explicit functions of time, explicit symplectic schemes [85] can be established. The most popular symplectic integrators are the second-order algorithms of Wisdom–Holman [86] and the fourth-order algorithms of Forest–Ruth [87]. In terms of the general second-order leapfrog methods, higher order symmetric integrators can be easily obtained according to the construction method of Yoshida [88]. Symplectic schemes conserve energy by making energy errors bounded and oscillating with evolution time. Unfortunately, not all Hamiltonian systems have such two explicitly integrable splitting forms. In this case, implicit symplectic methods [89,90] or implicit and explicit mixed symplectic methods [91–93] are available. Such implicit integrators need more computational cost than same-order standard explicit methods.

In the extended phase space method of Pihajoki [94], a new Hamiltonian consisting of two similar sub-Hamiltonians is provided to an inseparable Hamiltonian system. The two sub-Hamiltonians are both equal to the original Hamiltonian. The only difference is the combination of old variables intersecting with the new ones. Thus, the Hamiltonian systems with N-dimensional variables are doubled to 2N-dimension in its phase-space. Explicit symplectic methods can be taken because there is no canonical relationship between the old coordinates and the new momenta. Moreover, the coordinates or momenta in the extended phase space are projected back to the original space so as to keep the mixing maps of feedback between the two sub-Hamiltonian. Many references [71,95–97] show that extended phase space methods are well suited for various inseparable Hamiltonian problems. Luo [98] proved that midpoint permutations can maintain good long-term stability in energy errors. In general, mixing or projecting maps destroy symplectic properties; thus, the extended phase space algorithms are so-called as symplectic-like methods.

Recently, a class of explicit symplectic integrators was designed for black-hole spacetimes in general relativity [57,58,67–69,74,99]. By dividing the Hamiltonians or time-transformed Hamiltonian corresponding to the spacetimes into multiple parts, the authors used the analytical solutions of the splitting parts to compose a set of explicit symplectic integrators. Numerical tests indicate that these algorithms have high accuracy and Hamiltonian errors can be stabilized efficiently. However, the method for splitting the Hamiltonians is not universal [100]. It must rely on the terms composing of the Hamiltonians. There are various choices for specific problems. For example, the Hamiltonian of Schwarzschild black hole is separated into four integrable parts with explicit analytical solutions [67]. Similarly, the method is also available to five parts for Reissner–Nordström black hole [68], and six parts for Reissner–Nordström–(anti)-de Sitter black holes [69]. However, the above spitting method is not suitable for the Kerr speacetime. With the aid of the time transformation method introduced by Mikkola [101], Wu et al. [99] provided Kerr spacetime with a kind of time-transformed Hamiltonian with the desired splitting and successfully obtained explicit symplectic integrators. Such explicit symplectic integrators, with adaptive time steps, can achieve good long-term performances in the conservation of Hamiltonian quantities. This time-transform method is also suitable for the magnetized or deformed black holes [58,74].

On the other hand, only some stable circular orbits and some physical properties in the brane-world black hole spacetime were studied by the author of [6]. No one has studied how the positive cosmological and dark matter parameter affect the chaotic dynamics of charged particles although the chaotic motions have been well known already in many simpler situations. The study of such chaotic dynamics will be a possible reference for future studies of the brane-world black hole shadows with chaotic patterns of self-similar fractal structures based on the Event Horizon Telescope data for M87* and Sagittarius A*. Because of these points, we focus on the impacts of the positive cosmological and dark matter parameter on the chaotic dynamics of charged particles. This is another main aim of this paper. In summary, our main aims are to apply the proposed explicit symplectic integrators to study the dynamics of charged particles moving around the black hole with an external magnetic field. In particular, the effect of positive cosmological constant and dark matter parameter on the chaotic behavior is investigated.

The rest of this paper is organized as follows. In Section 2, we briefly introduce the brane-world black hole immersed in an axially external magnetic field. To explore the dynamics of charged particles, new explicit symplectic integrators are constructed. The numerical evaluation of the proposed integrators are presented in Section 3. Then, a fourth-order explicit symplectic integrator is applied to investigate the dynamics of charged particles. How chaotic motions depend on electromagnetic, cosmological, and dark matter parameters are discussed. Finally, the main results are concluded in Section 4.

2. Construction of Explicit Sympletic Intergrators in a Magnetized Brane-World Spacetime

Brane-world spacetimes [4–6] are a class of modified theories of gravity. In these brane-world models, gravitons can propagate through a bulk where ordinary matters (including human beings ourselves) are localized. One of the brane-world spacetimes [102,103] is not an asymptotically flat metric, which uses a confining potential rather than a delta-function in the energy-momentum tensor. The action of such a confining potential causes particles on a higher-dimensional model to be trapped on a four-dimensional hypersurface. In this brane theory, the covariant Einstein equations are based on the bulk equations projected onto the brane. There are two differences between the field equations on the brane and the Einstein equations in the standard model. One difference relates to high energies in the form of a new source term in the effective Einstein equation with the brane energy-momentum quadratic tensor. The other difference is the bulk having a non-vanishing Weyl-curvature projection onto the brane. Because of these points, the brane-world metric is suitable for studying solutions of compact sources on the brane such as stars and black holes. In particular, it is useful to account for the accelerated expansion of the universe and galaxy rotation curves.

2.1. Magnetized Brane-World Spacetime

In spherical-like coordinates, $\mathbf{x} = x^\mu$ corresponds to a four-dimensional coordinate vector $(x^0, x^1, x^2, x^3) = (t, r, \theta, \phi)$. A brane-world black hole [102] can be written as follows:

$$\begin{aligned} ds^2 &= g_{\mu\nu} dx^\mu dx^\nu \\ &= -g(r)dt^2 + g(r)^{-1}dr^2 + r^2(d\theta^2 + \sin^2\theta d\phi^2), \end{aligned} \tag{1}$$

where the coefficient function is written as follows.

$$g(r) = 1 - \frac{2M}{r} - \alpha^2 r^2 - 2\alpha\beta r - \beta^2. \tag{2}$$

Here, M is the mass of the black hole, and α and β are the cosmological and dark matter parameters. If the two parameters vanishes, line element (1) corresponds to the Schwarzschild metric, which has a horizon of $r = 2M$. The cosmological constant α responds to a weak-field gravity of galaxies, galaxy groups, and clusters. The alteration of the horizon with parameter α was discussed in [102]. In fact, without a large distance, the value of α is too small to affect the spacetime geometry [69]. The dark matter and dark energy may act as weak gravitational fields such as galaxies and galaxy groups or clusters [104,105]. With the aid of the luminosity function, Zwicky [106] predicted that more than half of all matter in the visible universe have been overlooked. The authors of [107] discussed the variation of the dark mass fraction in spiral galaxies. The authors of [108,109] determined the mass distribution in the galaxy by analyzing rotation curves and considered an amount of dark matter. Although there is no direct evidence of the presence of dark matter, theoretical analysis shows that the dark matter parameter may affect the motion of test particles [110]. Brane-world spacetime belongs to a modified theory of gravity. Of course, many other modified theories of gravity can be also be found in the literature [111–116].

The geodesic motion of a test particle is described by a Lagrangian:

$$\begin{aligned} \mathcal{L} &= \frac{1}{2}\left(\frac{ds}{d\tau}\right)^2 = \frac{1}{2} g_{\mu\nu}\dot{x}^\mu \dot{x}^\nu \\ &= \frac{1}{2}\left[-g(r)\dot{t}^2 + g(r)^{-1}\dot{r}^2 + r^2(\dot{\theta}^2 + \sin^2\theta\dot{\phi}^2)\right], \end{aligned} \tag{3}$$

where $\dot{x}$ denotes the derivative of variable x with respect to proper time τ. Geometric units are provided for the constant of gravity G and the speed of light c; that is, $c = G = 1$.

Taking $x \to xM$ and $\tau \to \tau M$, we have a dimensionless Lagrangian. For a time-like particle, the four-velocity vectors satisfies the following.

$$g_{\mu\nu}\dot{x}^{\mu}\dot{x}^{\nu} = -1. \tag{4}$$

Therefore, the Lagrangian always has the following constraint: $\mathcal{L} = -1/2$. By defining the following covariant generalized momentum:

$$P_{\mu} = \partial\mathcal{L}/\partial\dot{x}^{\mu} = g_{\mu\nu}\dot{x}^{\nu}, \tag{5}$$

we obtain the corresponding Hamiltonian.

$$\begin{aligned} \mathcal{H} &= P_{\mu}\dot{x}^{\mu} - \mathcal{L} = \frac{1}{2}g^{\mu\nu}P_{\mu}P_{\nu} \\ &= \frac{1}{2}\Big[-g(r)\dot{t}^2 + g(r)^{-1}\dot{r}^2 + r^2(\dot{\theta}^2 + \sin^2\theta\dot{\phi}^2)\Big]. \end{aligned} \tag{6}$$

Clearly, the Hamiltonian equals the Lagrangian.

Suppose the black hole is immersed in an external uniform magnetic field given by a four-vector potential that has only one nonzero covariant component:

$$A_{\phi} = \frac{B}{2}g_{\phi\phi} = \frac{B}{2}r^2\sin^2\theta, \tag{7}$$

where B is the constant strength of the uniform magnetic field. The magnetic field is too weak to change the metric of the spacetime, but it can considerably affect the motion of charged particles. Deng [6] showed that there are two horizons in the brane-world and discussed effective potential and periodic orbits. If a test particle with a charge q moves around this magnetized black hole, it has momentum $p_{\mu} = P_{\mu} + qA_{\mu}$. The Hamiltonian for the charged particle motion is determined by the following.

$$H = \frac{1}{2}g^{\mu\nu}(p_{\mu} - qA_{\mu})(p_{\nu} - qA_{\nu}). \tag{8}$$

This Hamiltonian does not explicitly contain the coordinates t and ϕ; therefore, the axially symmetric system has two conserved quantities of energy E and angular momentum L are defined as follows.

$$\begin{aligned} p_t &= P_t + qA_t = P_t = -g(r)\dot{t} = -E, \\ p_{\phi} &= P_{\phi} + qA_{\phi} = r^2\sin^2\theta\dot{\phi} + \frac{qB}{2}r^2\sin^2\theta = L. \end{aligned} \tag{9}$$

In terms of the two constants, the Hamiltonian can be simplified as follows.

$$\begin{aligned} H &= \frac{1}{2}\left[-\frac{E^2}{g(r)} + g(r)p_r^2 + \frac{1}{r^2}p_{\theta}^2 + \frac{(L - \frac{1}{2}qBr^2\sin^2\theta)^2}{r^2\sin^2\theta}\right] \\ &= \frac{1}{2}\left[\frac{-E^2}{1 - \frac{2}{r} - (\alpha r + \beta)^2} + \left(1 - \frac{2}{r} - (\alpha r + \beta)^2\right)p_r^2 + \frac{p_{\theta}^2}{r^2} + \frac{(L - \frac{1}{2}qBr^2\sin^2\theta)^2}{r^2\sin^2\theta}\right]. \end{aligned} \tag{10}$$

Due to the four-velocity or rest mass condition, the Hamiltonian also remains as follows.

$$H = -\frac{1}{2}. \tag{11}$$

2.2. Construction of Explicit Sympletic Intergrators

To investigate the dynamics of such a higher nonlinear system, we are required to employ good numerical integration methods. Symplectic integrators have good physical and geometric properties in the conservation of Hamiltonian flows and Hamiltonians and, therefore, are particularly suitable for the long-term evolution of Hamiltonian systems. The explicit symplectic methods have an advantage over the implicit one in terms of computational efficiency. Although the explicit symplectic methods in general relativity were recently designed by several authors [57,58,67–69,74,99,100], splitting Hamiltonians depends on different problems.

Following the previous works of Wang et al. [67–69], we can easily split the Hamiltonian (10) into five integrable parts:

$$H = H_1 + H_2 + H_3 + H_4 + H_5, \tag{12}$$

where all sub-Hamiltonians are written as follows.

$$H_1 = \frac{1}{2}\left[-\frac{E^2}{1-\frac{2}{r}-(\alpha r+\beta)^2} + \frac{(L-\frac{1}{2}qBr^2\sin^2\theta)^2}{r^2\sin^2\theta}\right], \tag{13}$$

$$H_2 = \frac{1}{2}p_r^2, \tag{14}$$

$$H_3 = -\frac{1}{r}p_r^2, \tag{15}$$

$$H_4 = -\frac{1}{2}(\alpha r+\beta)^2 p_r^2, \tag{16}$$

$$H_5 = \frac{1}{2r^2}p_\theta^2. \tag{17}$$

Hereafter, we take $b = qB$ as an electromagnetic parameter. For sub-Hamiltonian H_1, its canonical equations are $\dot{r} = \dot{\theta} = 0$ and the following.

$$\begin{aligned} \dot{p_r} &= \frac{dp_r}{d\tau} = -\frac{\partial H_1}{\partial r} = \Re(r,\theta), \\ \dot{p_\theta} &= \frac{dp_\theta}{d\tau} = -\frac{\partial H_1}{\partial \theta} = \Theta(r,\theta). \end{aligned} \tag{18}$$

It is clear that $r = r_0$ and $\theta = \theta_0$ when proper time proceeds from τ_0 to $\tau_1 = \tau_0 + h$, where h is a time step. Operator e^{hH_1} for the Equation (18) corresponds to explicit solutions:

$$\begin{aligned} e^{hH_1}: \quad & p_r = p_{r0} + h\Re(r_0,\theta_0), \\ & p_\theta = p_{\theta 0} + h\Theta(r_0,\theta_0), \end{aligned} \tag{19}$$

where r_0, θ_0, p_{r0}, and $p_{\theta 0}$ are the values of phase-space variables at initial time τ_0, and r, θ, p_r, and p_θ are those at time τ_1. The canonical equations of sub-Hamiltonians H_2, H_3, H_4, and H_5 have the following analytical solutions.

$$e^{hH_2}: r = r_0 + hp_{r0}, \tag{20}$$

$$\begin{aligned} e^{hH_3}: r &= [(r_0^2 - 3hp_{r0})^2/r_0]^{1/3}, \\ p_r &= p_{r0}(1 - 3hp_{r0}/r_0^2)^{1/3}, \end{aligned} \tag{21}$$

$$\begin{aligned} e^{hH_4}: r &= [(\alpha r_0 + \beta)e^{-h\alpha(\alpha r_0+\beta)p_{r0}} - \beta]/\alpha, \\ p_r &= p_{r0}e^{h\alpha(\alpha r_0+\beta)p_{r0}}, \end{aligned} \tag{22}$$

$$\begin{aligned} e^{hH_5}: \theta &= \theta_0 + hp_{\theta 0}/r_0^2, \\ p_r &= p_{r0} + hp_{r0}^2/r_0^3. \end{aligned} \tag{23}$$

Obviously, all the analytical solutions of the sub-Hamiltonians are explicit functions of proper time. Therefore, a second order symplectic integrator can be constructed as follows.

$$S2(h) = e^{\frac{h}{2}H_5}e^{\frac{h}{2}H_4}e^{\frac{h}{2}H_3}e^{\frac{h}{2}H_2} \circ e^{hH_1} \circ e^{\frac{h}{2}H_2}e^{\frac{h}{2}H_3}e^{\frac{h}{2}H_4}e^{\frac{h}{2}H_5}. \tag{24}$$

According to the idea of Yoshida [88], a ($2n$ + 2)th order integrator can be directly constructed with the combination of a symmetric integrator order $2n$:

$$S_{2n+2}(h) = S_{2n}(z_1 h) \circ S_{2n}(z_0 h) \circ S_{2n}(z_1 h), \tag{25}$$

where $z_0 = -\frac{2^{1/(2n+1)}}{2-2^{1/2(2n+1)}}$ and $z_1 = \frac{1}{2-2^{1/(2n+1)}}$. Using three second order symplectic integrators, we can easily obtain a fourth-order symplectic integrator $S4$.

3. Numerical Simulations

Considering the importance of symplectic integrators, we have proposed the fourth-order explicit symplectic integrator for simulating the motion of charged particles in a magnetized brane-world spacetime. The construction of such an integrator is based on a Hamiltonian for the spacetime separated into five parts, for which its solutions can be expressed as explicit functions of proper time. In this section, we mainly check the numerical performance of the explicit symplectic integrator and consider the application of this integrator to the study of orbital dynamics.

3.1. Performance Evaluation of the Explicit Sympletic Intergrators

Given parameters $\alpha = 10^{-12}$, $\beta = 0$, and $b = 0$, the problem corresponds to a Schwarzschild black hole with a cosmic background. Considering the accelerated expansion of the universe [117–119], we set the cosmological parameter as a positive constant. The energy and angular momentum are $E = 0.9900, L = 4.6$, and the proper time step is $h = 1$. Initial conditions are $\theta = \pi/2, p_r = 0, r = 10$, and the starting value of $p_\theta(> 0)$ is determined by Equations (10) and (11). As shown by the second-order method S2 in Figure 1a, the loop colored red in the Poincaré section at plane $\theta = \pi/2$ and $p_\theta > 0$ indicates a regular quasi-periodic orbit. Similarly, other orbits with initial separations $r = 15, 30, 40, 50, 65$ are also regular. These results are consistent with the integrability of the Hamiltonian system without external magnetic field. This integrability is because the system has four conserved quantities including the particle energy, angular momentum, rest mass, and azimuthal motion [99,120]. Three Hamiltonian errors of the second-order algorithms are significantly different, as shown in Figure 1b. For explicit symplectic method $S2$, it has good stability and can remain bounded in an order of 10^{-7}. The extended phase-space method $EE2$ [67] has a secular drift in Hamiltonian errors. The Hamiltonian errors of explicit and implicit mixed symplectic method $EI2$ [67] are an order of magnitude larger than $S2$ and $EE2$, as listed in Table 1. This is due to a poor iteration precision. Computational costs are listed in Table 2, where the CPU time of method $EI2$ costs nearly at a double than that for method $S2$. Figure 1c describes that the Hamiltonian errors of the conventional fourth-order Runge–Kutta method $RK4$ reach an order of 10^{-7} and increase linearly with time. Unlike method $RK4$ and the fourth-order explicit and implicit mixed symplectic method $EI4$, the fourth-order extended phase space and explicit symplectic-like method $EE4$ [67] and the new fourth-order explicit symplectic method $S4$ are accurate to an order of 10^{-10}. Distinct from the second-order algorithms, $EE4$, $EI4$, and $S4$ exhibit excellent stability in the errors, as shown in Figure 1d. However, the Hamiltonian errors of $EI4$ are still several orders of magnitude larger than those of $EE4$ and $S4$.

Table 1. Computational accuracy of different algorithms. Largest absolute values of Hamiltonian errors correspond to time step h. Orbit 1 is integrated until proper time $\tau = 10^8$.

Method	EI2	EE2	S2	RK4	EI4	EE4	S4
h = 1	1.8×10^{-5}	1.2×10^{-6}	5×10^{-7}	6×10^{-7}	6×10^{-5}	7×10^{-10}	3×10^{-10}
h = 0.1	7×10^{-6}	1.5×10^{-9}	5×10^{-10}	6×10^{-12}	2×10^{-6}	1×10^{-13}	8×10^{-13}

Table 2. Same as Table 1. Computational cost, i.e., CPU times (seconds), for algorithms.

Method	EI2	EE2	S2	RK4	EI4	EE4	S4
h = 1	64.98	17.28	25.56	20.06	362.16	49.92	75.20
h = 0.1	317.56	155.53	276.98	208.11	853.83	503.08	763.02

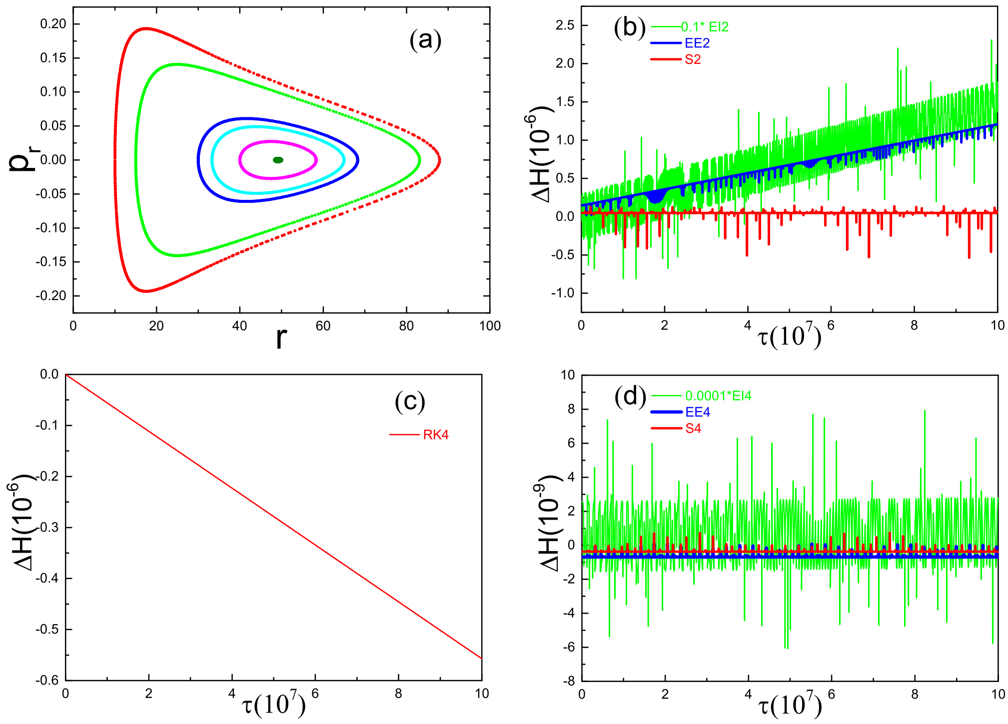

Figure 1. Numerical test performance. (**a**) Poincaré sections on the plane $\theta = \pi/2$. The parameters are $E = 0.9900, L = 4.6, \alpha = 10^{-12}, \beta = 0, b = 0$. Initial conditions of orbit 1 colored red are $r = 10$, $p_r = 0$, $\theta = \pi/2$, and p_θ is determined by Equations (11) and (12). The other orbits are $r = 15, 30, 40, 50$ and $r = 65$. (**b**–**d**) Hamiltonian errors $\Delta H = H - (-1/2)$ of orbit 1 for different algorithms. The proper time step is $h = 1$.

Clearly, the symplectic integrators have good physical and geometric properties in the conservation of Hamiltonian flows and Hamiltonians and, therefore, are particularly suitable for the long-term evolution of Hamiltonian systems. The explicit symplectic methods have an advantage over the implicit one in terms of computational efficiency.

We employed an explicit symplect algorithm *S*4 with time step $h = 1$ for later calculations.

3.2. Dependence of the Orbital Dynamics on the Parameters

Since numerical experiments show that Hamiltonian errors remain bounded for long-term integrations of orbits by the proposed symplectic integrator. The fourth-order explicit symplectic algorithm with an appropriate step size is applied to explore the dynamics of charged particles. In what follows, the dependence of the chaotic behavior on the electromagnetic parameter, cosmological constant, and dark matter parameter is surveyed.

3.2.1. Orbital Dynamics Influenced by the Electromagnetic Parameter

The parameters are the same as those in Figure 1, with the exception that the electromagnetic parameter increases slightly. When $b = 0.0015$, the orbits corresponding to initial separations r = 10, 15, 30, 40, 50 and $r = 65$ in Figure 2a are regular KAM loops. These smooth curves in the Poincaré section indicates that the motions of the orbits are quasi-periodic. If the electromagnetic parameter becomes a little large, then $b = 0.0020$. As shown in panel (b), there are two KAM loops with an initial orbit condition $r = 30, 50$

(colored blue and olive) replaced by several separate islands. There are many random discrete points (colored cyan) in the phase diagram when the orbit takes an initial value of $r = 65$. This indicates that the regularity of the orbit is broken. That is to say that the motion of the test particle becomes weakly chaotic. With a further increase in the electromagnetic parameter, e.g., $b = 0.0024$, many orbits ($r = 30, 50, 65$) turn out to be chaotic in panel (c). In fact, the extent of chaos is also strengthened. Given electromagnetic parameter $b = 0.0025$, the chaotic motions of test particles are filled in a large region, as shown in panel (d).

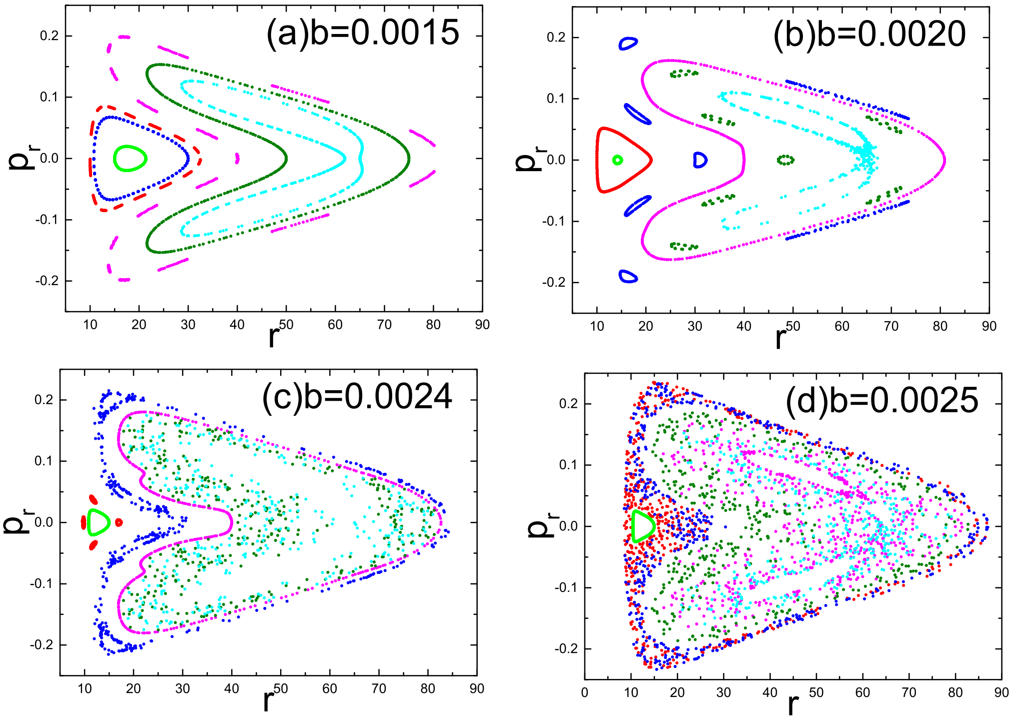

Figure 2. Dependence of the orbital dynamics on electromagnetic parameter b. Poincaré sections with the same parameters $E = 0.9900, L = 4.6, \alpha = 10^{-12}, \beta = 0$, and different positive values of electromagnetic parameter b are given. The orbits are same as in Figure 1.

From the above discussion, we can see that chaos should become strong as magnetic field parameter b increases. The result fits well with that in the previous references [59–61,67–71,75,76]. These facts show that the external electromagnetic forces lead to an absence of the fourth constant (i.e., the azimuthal motion), and they are an important source for inducing chaos. However, not all external electromagnetic fields must admit the onset of chaotic motion. Recently, the authors of [121] proved the integrability of charged particles by moving around the Kerr–Newman black hole surrounded by cloud strings, quintessence, and an electromagnetic field. If the cosmological constant Λ included in the model is nonvanishing, then the fourth constant is absent and chaos may occur. It is different from brane-world spacetime.

3.2.2. Orbital Dynamics Influenced by the Cosmological Parameter

The cosmological and dark matter but the magnetic field parameter can decide whether the system is chaotic. It is still meaningful to study how the cosmological constant or the dark matter parameter exerts an influence on chaos. Now, we fix parameters $E = 0.9900, L = 3.7, \beta = 0$, and $b = 0.0012$. The initial separations of orbits are $r = 10, 15, 50, 60, 65$ and $r = 80$. For the case of $\alpha = 3 \times 10^{-6}$, three chaotic orbits ($r = 10, 60, 65$, colored red, magenta, and olive, respectively) exist in Figure 3a. Panels (b), (c), and (d) correspond to parameters $\alpha = 4 \times 10^{-6}, 5 \times 10^{-6}$, and 7×10^{-6}, respectively. The diagrams in panels (b)–(d) are similar to those in Figure 3a. In fact, the extent of chaos is gradually intensified as the cosmological parameter increases. For example, projective dots ($r = 10$, colored red) in the Poincaré section tend to become more and more discrete. This indicates the chaotic motion of the system, which becomes more dramatic. Obviously, an increase in the positive cosmological constant can strengthen the degree of chaos from the global phase-space structure.

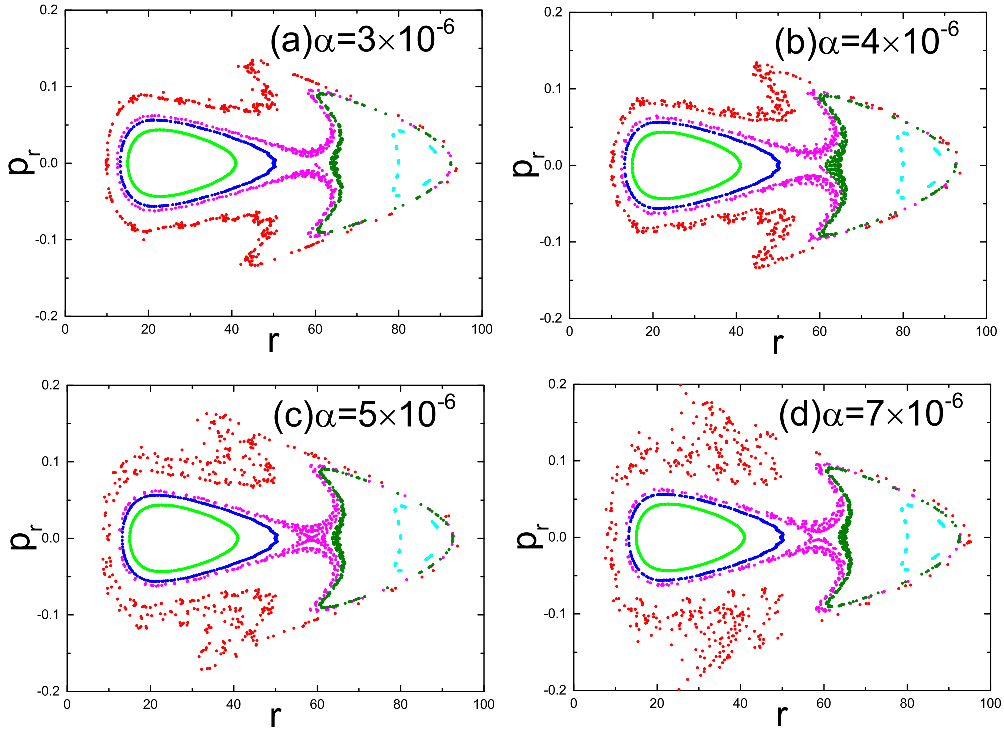

Figure 3. Dependence of the orbital dynamics on the cosmological parameter α. Poincaré sections with the same parameters $E = 0.9900, L = 3.7, b = 0.0012, \beta = 0$, and different values of cosmological parameter α are given. The orbits are $r = 10, 15, 50, 60, 65, 80$.

3.2.3. Orbital Dynamics Influenced by the Dark Matter Parameter

Finally, let us focus on what orbital dynamics will occur if dark matter parameter β increases. The fixed parameters are $E = 0.9900, L = 4.1, \alpha = 10^{-7}$, and $b = 0.0012$. Here the orbits have initial values $r = 10, 15, 50, 55, 65$ and $r = 80$. Figure 4a–f describe how chaotic motion evolves when the dark matter parameter gradually increases from $\beta = 1 \times 10^{-2}$ to 8×10^{-2}. Despite the fact that the orbital motions of $r = 10$ (colored red) return to the order starting after chaotic processes, the chaotic properties can be enhanced from the global phase space structure with an increasing dark matter parameter.

3.3. Explanation to the Influences of the Parameters on Chaotic Behavior

As is demonstrated above, the extent of chaos can be strengthened with a increase in the electromagnetic parameter, the positive cosmological constant or the dark matter parameter. The effects of the parameters on the chaotic dynamics can be explained as follows. We expand term $()^{-1}$ in Equation (13) and rewrite it as follows.

$$H_1 = -\frac{1}{2}[(1+\beta^2+8\alpha\beta)E^2 + bL] + \frac{1}{8}br^2\sin^2\theta - \frac{1}{2}\alpha^2E^2r^2 \\ -\alpha(2\alpha+\beta)E^2r - \frac{E^2}{r} - \frac{2\beta^2E^2}{r} + \frac{L^2}{2r^2\sin^2\theta} + ... \tag{26}$$

If $\alpha = 0, \beta = 0$, and $b = 0$, the fifth term of Equation (26) corresponds to a gravitational field. The test particles that suffered only involved gravity in Schwarzschild spacetime, which is oriented towards the black hole in Figure 5a. The cosmological parameter in the third term of Equation (26) has a gravitational repulsive force from the galaxies and galaxy groups or clusters, which can directly act on the particles. It weakens the gravitational force effect from the center object, as shown in Figure 5b. The positive dark matter parameter in the sixth term of Equation (26) also yields a gravitational force. It enhances the gravity of the black hole, as shown in Figure 5c. Compared with the forces from the cosmological parameter, the gravitational attraction of the central object has overwhelming dominance. For this case, without external magnetic fields, the motions of test particles are always regular even if the cosmological and dark matter parameters are involved. Unlike the cosmological and dark matter parameters in the metric, the electromagnetic parameter in the second term of Equation (26) corresponds to an external force. The Lorentz force acting on a charged particle is attractive towards the black hole when $b > 0$, as shown in Figure 5d. Chaos may only occur when the gravitational field from the black hole and the magnetic field are approximately balanced. Namely, the Lorentz force can induce chaos in some cases when it is strong enough.

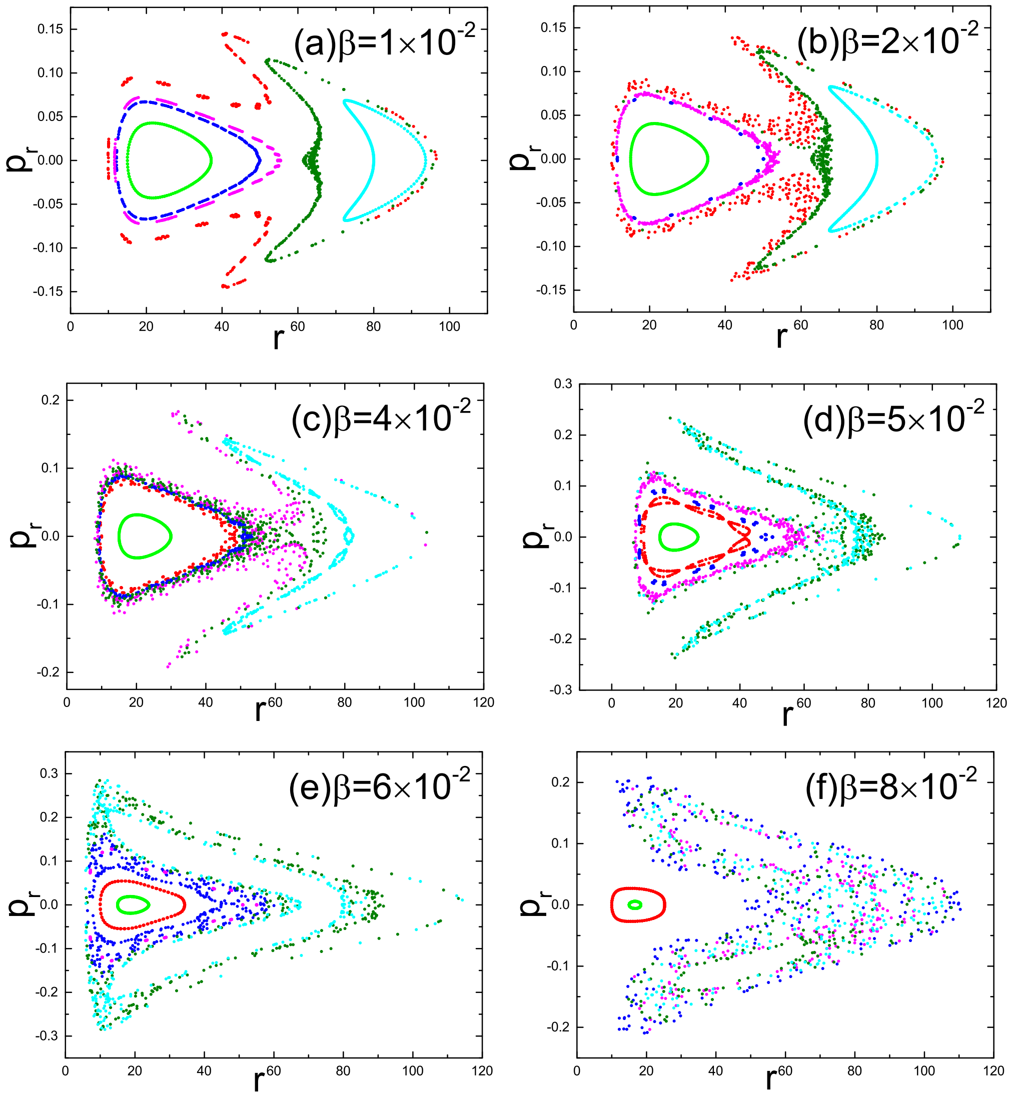

Figure 4. Dependence of the orbital dynamics on the dark matter parameter β. Poincaré sections with the same parameters $E = 0.9900, L = 4.1, b = 0.0012, \alpha = 10^{-7}$, and different values of dark matter parameter β are given. The corresponding orbits are $r = 10, 15, 50, 55, 65, 80$.

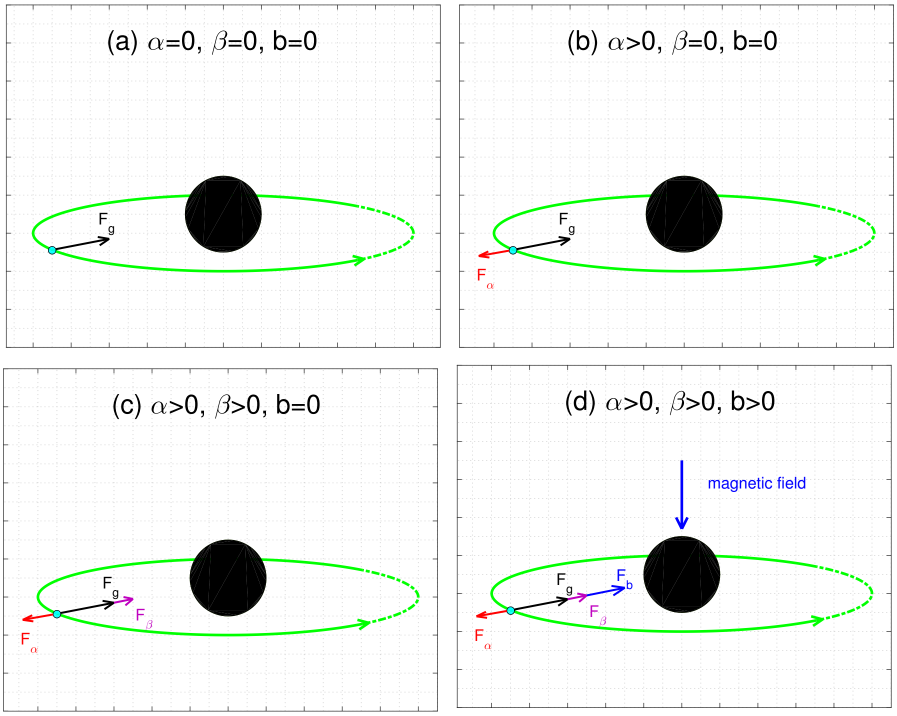

Figure 5. Representation of the force responding to the parameters. Case (**a**) refers to a test particle moving around Schwarzschild black hole, and the particle only suffers gravity F_g from the central object. Case (**b**) refers to the Schwarzschild black hole with a cosmological background, and repulsive force F_α is the resultant action from the gravity of galaxies and galaxy groups or clusters. Case (**c**) considers the appearance of dark matter, and force F_β is an effect of the gravitational force of dark matter. Case (**d**) describes the spacetime immersed in an axially magnetic field, and Lorentz force F_b acts on charged particle additionally.

As a result, the magnetic field determines whether the motion of particles is chaotic, and the extent of chaos may become strong when the electromagnetic parameter increases. The presence of cosmological constant weakens the gravity of the black hole; equivalently, the electromagnetic force increases. That is why the extent of chaos is strengthened when the cosmological constant increases.

4. Summary

In this work, we set up a fourth-order explicit symplectic integrator for the dynamics of charged particles around the magnetized brane-world black hole. The construction of such an integrator requires the Hamiltonian corresponding to this spacetime to be separated into five parts with analytical solutions, and this can be expressed as explicit functions of proper time. Numerical tests show that the proposed algorithm performs good performance for long-term integrations of orbits.

Then, the new fourth-order explicit symplectic integrator is employed to study the effect of the different parameters contributing to chaos. Electromagnetic parameter corresponds to the Lorentz force acting on the charged particles. It can destroy the integrability of the Hamiltonian system without an electromagnetic force and admits the onset of chaos. Dark matter acts as a gravitational force, which agrees with the electromagnetic parameter, and chaotic motion can become more obvious when dark matter increases. The gravity of the black hole is weakened with an increasing positive cosmological parameter; therefore, the extent of chaos can be also strengthened.

In future work, we shall focus on how the positive cosmological and dark matter parameter affect brane-world black hole shadows. They will be estimated based on the Event Horizon Telescope data for M87* and Sagittarius A*. We shall establish a ray-tracing code using the proposed symplectic integrator. The ray-tracing code and the study of such chaotic dynamics will be used to explore the effects of chaos on brane-world black hole shadows.

Author Contributions: Conceptualization, methodology, and supervision, G.H.; software and writing—original draft, A.H. All authors have read and agreed to the published version of the manuscript.

Funding: This research has been supported by the National Natural Science Foundation of China (Grant No. 11533004 and 11663005) and the Natural Science Foundation of Jiangxi province (Grant No. 2016BAB201015).

Institutional Review Board Statement: Not applicable.

Informed Consent Statement: Not applicable.

Data Availability Statement: Not applicable.

Acknowledgments: The authors are very grateful to Wu Xin for valuable suggestions. They also thank the referees for useful suggestions.

Conflicts of Interest: The authors declare no conflict of interest.

References

1. The Event Horizon Telescope Collaboration. First M87 Event Horizon Telescope Results. I. The Shadow of the Supermassive Black Hole. *Astrophys. J. Lett.* **2019**, *875*, L1. [CrossRef]
2. The Event Horizon Telescope Collaboration. First M87 Event Horizon Telescope Results. VII. Polarization of the Ring. *Astrophys. J. Lett.* **2021**, *910*, 12. [CrossRef]
3. Abbott, B.P.; Abbott, R.; Abbott, T.D.; Abernathy, M.R.; Acernese, F.; Ackley, K.; Adams, C.; Adams, T.; Addesso, P.; Adhikari, R.X.; et al. Observation of Gravitational Waves from a Binary Black Hole Merger. *Phys. Rev. Lett.* **2016**, *116*, 061102. [CrossRef]
4. Arkani-Hamed, N.; Dimopoulos, S.; Dvali, G. The Hierarchy Problem and New Dimensions at a Millimeter. *Phys. Lett. B* **1998**, *429*, 263–272. [CrossRef]
5. Randall, L.; Sundrum, R. An Alternative to Compactification. *Phys. Rev. Lett.* **1999**, *83*, 4690–4693. [CrossRef]
6. Deng, X.M. Periodic orbits around brane-world black holes. *Eur. Phys. J. C* **2020**, *80*, 489. [CrossRef]
7. Brans, C.; Dicke, R.H. Mach's Principle and a Relativistic Theory of Gravitation. *Phys. Rev.* **1961**, *124*, 925. [CrossRef]
8. Brans, C. Mach's Principle and a Relativistic Theory of Gravitation. II. *Phys. Rev.* **1961**, *125*, 2194. [CrossRef]
9. Chen, X.; Kamionkowski, M. Cosmic microwave background temperature and polarization anisotropy in Brans-Dicke cosmology. *Phys. Rev. D* **1999**, *60*, 104036. [CrossRef]
10. Damour, T.; Nordtvedt, K. General relativity as a cosmological attractor of tensor-scalar theories. *Phys. Rev. Lett.* **1993**, *70*, 2217–2219. [CrossRef]
11. Minas, G.; Saridakis, E.N.; Stavrinos, P.C.; Triantafyllopoulos, A. Bounce Cosmology in Generalized Modified Gravities. *Universe* **2019**, *5*, 74. [CrossRef]
12. Deng, X.; Xie, Y. Solar System tests of a scalar-tensor gravity with a general potential: Insensitivity of light deflection and Cassini tracking. *Phys. Rev. D* **2016**, *93*, 044013. [CrossRef]
13. Deng, X. Two-post-Newtonian approximation of the scalar-tensor theory with an intermediate-range force for general matter. *Sci. China Phys. Mech. Astron.* **2015**, *58*, 1–8. [CrossRef]
14. Deng, X.M.; Xie, Y. Two-post-Newtonian light propagation in the scalar-tensor theory: An N-point mass case. *Phys. Rev. D* **2012**, *86*, 044007. [CrossRef]
15. Deng, X.M. Constraints on a scalar-tensor theory with an intermediate-range force by binary pulsars. *Sci. China G: Phys. Astron.* **2011**, *54*, 2071. [CrossRef]
16. Gong, Y.; Papantonopoulos, E.; Yi, Z. Constraints on scalar-tensor theory of gravity by the recent observational results on gravitational waves. *Eur. Phys. J. C* **2018**, 78, 738. [CrossRef]
17. Jacobson, T. Einstein-æther gravity: A status report. *Proc. Sci. (Quantum Emergent Gravity Theory Phenomenol.)* **2007**, 43, 020.
18. Rosen, N. General relativity and flat space. II. *Phys. Rev.* **1940**, *57*, 150–153. [CrossRef]
19. Rosen, N. A bi-metric theory of gravitation. *Gen. Relativ. Gravit.* **1973**, *4*, 435–447. [CrossRef]
20. Drummond, I.T. Bimetric gravity and "dark matter". *Phys. Rev. D* **2001**, *63*, 043503. [CrossRef]
21. Tamaki, T. Post-Newtonian parameters in the tensor-vector-scalar theory. *Phys. Rev. D* **2008**, *77*, 124020. [CrossRef]
22. Lasky, P.D.; Sotani, H.; Giannios, D. Structure of neutron stars in tensor-vector-scalar theory. *Phys. Rev. D* **2008**, *78*, 104019. [CrossRef]
23. Skordis, C. The tensor-vector-scalar theory and its cosmology. *Class. Quantum Grav.* **2009**, *26*, 143001. [CrossRef]
24. Freire, P.C.C.; Wex, N.; Esposito-Farèse, G.; Verbiest, J.P.W.; Bailes, M.; Jacoby, B.A.; Kramer, M.; Stairs, I.H.; Antoniadis, J.; Janssen, G.H. The relativistic pulsar-white dwarf binary PSR J1738+0333—II. The most stringent test of scalar-tensor gravity. *Mon. Not. R. Astron. Soc.* **2012**, *423*, 3328–3343. [CrossRef]

25. Moffat, J.W. Scalar-tensor-vector gravity theory. *J. Cosmol. Astropart. Phys.* **2006**, *3*, 4. [CrossRef]
26. Deng, X.M.; Xie, Y.; Huang, T.Y. Modified scalar-tensor-vector gravity theory and the constraint on its parameters. *Phys. Rev. D* **2009**, *79*, 044014. [CrossRef]
27. Hehl, F.W.; Von der Heyde, P.; Kerlick, G.D.; Nester, J.M. General relativity with spin and torsion: Foundations and prospects. *Rev. Mod. Phys.* **1976**, *48*, 393. [CrossRef]
28. Trautman, A. Einstein-Cartan theory. *Encycl. Math. Phys.* **2006**, *2*, 189–195.
29. Capozziello, S.; Nojiri, S.; Odintsov, S.D.; Troisi, A. Cosmological viability of f(R)-gravity as an ideal fluid and its compatibility with a matter dominated phase. *Phys. Lett. B* **2006**, *639*, 135. [CrossRef]
30. Sotiriou, T.P.; Faraoni, V. f(R) theories of gravity. *Rev. Mod. Phys.* **2010**, *82*, 451–497. [CrossRef]
31. Nojiri, S.I.; Odintsov, S.D. Unified cosmic history in modified gravity: From F(R) theory to Lorentz non-invariant models. *Phys. Rep.* **2011**, *505*, 59–144. [CrossRef]
32. De Felice, A.; Gérard, J.M.; Suyama, T. Cosmological perturbation in f(R,G) theories with a perfect fluid. *Phys. Rev. D* **2010**, *82*, 063526.
33. Deng, X.M.; Xie, Y. Solar System's Bounds on the Extra Acceleration of f(R, T) Gravity Revisited. *Int. J. Theor. Phys.* **2015**, *54*, 1739–1749. [CrossRef]
34. Felice, A.D.; Tsujikawa, S. Construction of cosmologically viable f(G) gravity models. *Phys. Lett. B* **2009**, *675*, 1–8. [CrossRef]
35. Deng, X.M.; Xie, Y. Improved Solar System bounds on the cosmologically viable f(G) gravity. *Astrophys. Space Sci.* **2017**, *362*, 59. [CrossRef]
36. Silva, M.V.d.S.; Rodrigues, M.E. Regular black holes in f(G) gravity. *Eur. Phys. J. C* **2018**, *78*, 638. [CrossRef]
37. Hořava, P. Quantum gravity at a Lifshitz point. *Phys. Rev. D* **2009**, 79, 084008.
38. Hořava, P. Spectral dimension of the universe in quantum gravity at a Lifshitz point. *Phys. Rev. Lett.* **2009**, *102*, 161301. [CrossRef]
39. Wang, A. Vector and tensor perturbations in Horava-Lifshitz cosmology. *Phys. Rev. D* **2010**, *82*, 124063. [CrossRef]
40. Chow, N.; Khoury, J. Galileon Cosmology. *Phys. Rev. D* **2009**, *80*, 024037. [CrossRef]
41. Ali, A.; Gannouji, R.; Sami, M. Modified gravity à la Galileon: Late time cosmic acceleration and observational constraints. *Phys. Rev. D* **2010**, *82*, 103015. [CrossRef]
42. Appelquist, T.; Chodos, A. Quantum Effects in Kaluza-Klein Theories. *Phys. Rev. Lett.* **1983**, *50*, 141. [CrossRef]
43. Overduin, J.M.; Wesson, P.S. Kaluza-Klein gravity. *Phys. Rep.* **1997**, *283*, 303–380. [CrossRef]
44. Deng, X.M.; Xie, Y. Improved upper bounds on Kaluza-Klein gravity with current Solar System experiments and observations. *Eur. Phys. J. C* **2015**, *75*, 539. [CrossRef]
45. Langlois, D.; Maartens, R.; Wands, D. Gravitational waves from inflation on the brane. *Phys. Lett. B* **2000**, *489*, 259–267. [CrossRef]
46. Neronov, A.; Sachs, I. On metric perturbations in brane-world scenarios. *Phys. Lett. B* **2001**, *513*, 173–178. [CrossRef]
47. Bostock, P.; Gregory, R.; Navarro, I.; Santiago, J. Einstein gravity on the codimension 2-brane? *Phys. Rev. Lett.* **2004**, *92*, 221601. [CrossRef]
48. Charmousis, C.; Zegers, R. Einstein gravity on an even codimension brane. *Phys. Rev. D* **2005**, *72*, 064005. [CrossRef]
49. Kobayashi, T.; Shiromizu, T.; Deruelle, N. Low energy effective gravitational equations on a Gauss-Bonnet brane. *Phys. Rev. D* **2006**, *74*, 104031. [CrossRef]
50. Zipoy, D.M. Topology of Some Spheroidal Metrics. *J. Math. Phys.* **1966**, *7*, 1137. [CrossRef]
51. Voorhees, B.H. Static Axially Symmetric Gravitational Fields. *Phys. Rev. D* **1970**, *2*, 2119. [CrossRef]
52. Psaltis, D.; Perrodin, D.; Dienes, K.R.; Mocioiu, I. Kerr Black Holes Are Not Unique to General Relativity. *Phys. Rev. Lett.* **2008**, *100*, 091101. [CrossRef] [PubMed]
53. Schwarzschild, K. On the Gravitational Field of a Mass Point according to Einstein's Theory. *Stizber. Deut. Akad. Wiss. Math. Phys.* **1916**, 89–196.
54. Reissner, H. On the Eigengravitation of the electric Fields according to the Einstein Theory. *Annalen der Physik* **1916**, *50*, 106. [CrossRef]
55. Nordström, G. On the energy of the gravitation field in Einstein's theory. *Proc. Kon. Ned. Akad. Wet.* **1918**, *20*, 1238.
56. Kerr, R.P. Gravitational field of a spinning mass as an example of algebraically special metrics. *Phys. Rev. Lett.* **1963**, *11*, 237–238. [CrossRef]
57. Sun, W.; Wang, Y.; Liu, Y.F.; Wu, X. Applying explicit symplectic integrator to study chaos of charged particles around magnetized Kerr black hole. *Eur. Phys. J. C* **2021**, *81*, 785. [CrossRef]
58. Sun, X.; Wu, X.; Wang, Y.; Deng, C.; Liu, B.R.; Liang, E.W. Dynamics of Charged Particles Moving around Kerr Black Hole with Inductive Charge and External Magnetic Field. *Universe* **2021**, *7*, 410. [CrossRef]
59. Hu, A.R.; Huang, G.Q. Dynamics of charged particles in the magnetized γ spacetime. *Eur. Phys. J. Plus.* **2021**, *136*, 1210. [CrossRef]
60. Yang, D.; Cao, W.; Zhou, N.; Zhang, H.; Liu, W.; Wu, X. Chaos in a Magnetized Modified Gravity Schwarzschild Spacetime. *Universe* **2022**, *8*, 320. [CrossRef]
61. Polcar, L.; Semerák, O. Free motion around black holes with discs or rings: Between integrability and chaos. VI. The Melnikov method. *Phys. Rev. D* **2019**, *100*, 103013. [CrossRef]
62. Wu, X.; Zhang, H. Chaotic dynamics in a superposed Weyl spacetime. *Astrophys. J.* **2006**, 652, 1466. [CrossRef]
63. Stuchlík, Z.; Kološ, M. Acceleration of the charged particles due to chaotic scattering in the combined black hole gravitational field and asymptotically uniform magnetic field. *Eur. Phys. J. C* **2016**, *76*, 32. [CrossRef]

64. Cunha, P.V.P.; Herdeiro, C.A.R.; Radu, E.; Rúnarsson, H.F. Shadows of Kerr Black Holes with Scalar Hair. *Phys. Rev. Lett.* **2015**, *115*, 211102. [CrossRef]
65. Cunha, P.V.P.; Grover, J.; Herdeiro, C.; Radu, E.; Rúnarsson, H.; Wittig, A. Chaotic lensing around boson stars and Kerr black holes with scalar hair. *Phys. Rev. D* **2016**, *94*, 104023. [CrossRef]
66. Takahashi, M.; Koyama, H. Chaotic motion of charged particles in an electromagnetic field surrounding a rotating black hole. *Astrophys. J.* **2009**, *693*, 472–485. [CrossRef]
67. Wang, Y.; Sun, W.; Liu, F.Y.; Wu, X. Construction of Explicit Symplectic Integrators in General Relativity. I. Schwarzschild Black Holes. *Astrophys. J.* **2021**, *907*, 66. [CrossRef]
68. Wang, Y.; Sun, W.; Liu, F.Y.; Wu, X. Construction of Explicit Symplectic Integrators in General Relativity. II. Reissner-Nordstrom Black Holes. *Astrophys. J.* **2021**, 909, 22. [CrossRef]
69. Wang, Y.; Sun, W.; Liu, F.Y.; Wu, X. Construction of Explicit Symplectic Integrators in Gen-eral Relativity. III. Reissner-Nordstrom-(anti)-de Sitter Black Holes. *Astrophys. J. Suppl. Ser.* **2021**, *254*, 8. [CrossRef]
70. Karas, V.; Vokrouhlický, D. Chaotic motion of test particles in the Ernst space-time. *Gen. Relativ. Gravit.* **1992**, *24*, 729–743. [CrossRef]
71. Li, D.; Wu, X. Chaotic motion of neutral and charged particles in a magnetized Ernst-Schwarzschild spacetime. *Eur. Phys. J. Plus.* **2019**, *134*, 96. [CrossRef]
72. Lukes-Gerakopoulos, G. The non-integrability of the Zipoy-Voorhees metric. *Phys. Rev. D* **2012**, *86*, 044013. [CrossRef]
73. Yi, M.; Wu, X. Dynamics of charged particles around a magnetically deformed Schwarzschild black hole. *Phys. Scr.* **2020**, *95*, 085008. [CrossRef]
74. Zhang, H.X.; Zhou, N.Y.; Liu, W.F.; Wu, X. Charged Particle Motions near Non-Schwarzschild Black Holes with External Magnetic Fields in Modified Theories of Gravity. *Universe* **2021**, *7*, 488. [CrossRef]
75. Nacozy, P.E. The use of integrals in numerical integrations of the N-body problem. In *International Astronomical Union Colloquium*; Cambridge University Press: Cambridge, UK, 1971; Volume 10, p. 40.
76. Fukushima, T. Efficient orbit integration by dual scaling for consistency of Kepler energy and Laplace integral. *Astron. J.* **2003**, *126*, 2567. [CrossRef]
77. Ma, D.Z.; Wu, X.; Zhu, J.F. Velocity scaling method to correct individual Kepler energies. *New Astron.* **2008**, *13*, 216–223. [CrossRef]
78. Wang, S.C.; Wu, X.; Liu, F.Y. Implementation of the velocity scaling method for elliptic restricted three-body problems. *Mon. Not. R. Astron. Soc.* **2016**, *463*, 1352. [CrossRef]
79. Wang, S.C.; Huang, G.Q.; Wu, X. Simulations of dissipative circular restricted three-body problems using the velocity-scaling correction method. *Astron. J.* **2018**, 155, 67. [CrossRef]
80. Deng, C.; Wu, X.; Liang, E.W. The use of Kepler solver in numerical integrations of quasi-Keplerian orbits. *Mon. Not. R. Astron. Soc.* **2020**, *496*, 2946–2961. [CrossRef]
81. Chorin, A.; Huges, T.J.; McCracken, M.F.; Marsden, J.E. Product formulas and numerical algorithms. *Commun. Pure Appl. Math.* **1978**, *31*, 205–256. [CrossRef]
82. Hu, S.Y.; Wu, X.; Huang, G.Q.; Liang, E.W. A Novel Energy-conserving Scheme for Eight-dimensional Hamiltonian Problems. *Astrophys. J.* **2019**, *887*, 191. [CrossRef]
83. Hu, S.Y.; Wu, X.; Liang, E.W. An Energy-conserving Integrator for Conservative Hamiltonian Systems with Ten-dimensional Phase Space. *Astrophys. J. Suppl. Ser.* **2021**, *235*, 55. [CrossRef]
84. Hu, S.Y.; Wu, X.; Liang, E.W. Construction of second-order six-dimensional Hamiltonian-conserving scheme. *Astrophys. J. Suppl. Ser.* **2021**, *257*, 40. [CrossRef]
85. Zhang, L.; Wu, X.; Liang, E. Adjustment of Force-Gradient Operator in Symplectic Methods. *Mathematics* **2021**, *9*, 2718. [CrossRef]
86. Wisdom, J.; Holman, M. Symplectic maps for the n-body problem. *Astron. J.* **1991**, *102*, 1528–1538. [CrossRef]
87. Forest, E.; Ruth, R.D. Fourth-order symplectic integration. *Physica D* **1990**, *43*, 105–117. [CrossRef]
88. Yoshida, H. Construction of higher order symplectic integrators. *Phys. Lett. A* **1990**, *150*, 262–268. [CrossRef]
89. Feng, K. Symplectic Geometry and Numerical Methods in Fluid Dynamics. In *Tenth International Conference on Numerical Methods in Fluid Dynamics. Lecture Notes in Physics*; Springer: Berlin/Heidelberg, Germany, 1986; Volume 264, pp. 1–7.
90. Brown, J.D. Midpoint rule as a variational-symplectic integrator: Hamiltonian systems. *Phys. Rev. D* **2006**, *73*, 024001. [CrossRef]
91. Liao, X.H. Symplectic integrator for general near-integrable Hamiltonian system. *Celest. Mech. Dyn. Astron.* **1997**, *66*, 243–253. [CrossRef]
92. Lubich, C.; Walther, B.; Brügmann, B. Symplectic integration of post-Newtonian equations of motion with spin. *Phys. Rev. D* **2010**, *81*, 104025. [CrossRef]
93. Zhong, S.Y.; Wu, X.; Liu, S.Q.; Deng, X.F. Global symplectic structure-preserving integrators for spinning compact binaries. *Phys. Rev. D* **2010**, *82*, 124040. [CrossRef]
94. Pihajoki, P. Explicit methods in extended phase space for inseparable Hamiltonian problems. *Celest. Mech. Dyn. Astron.* **2015**, *121*, 211–231. [CrossRef]
95. Liu, L.; Wu, X.; Huang, G.Q.; Liu, F.Y. Higher order explicit symmetric integrators for inseparable forms of coordinates and momenta. *Mon. Not. R. Astron. Soc.* **2016**, *459*, 1968–1976. [CrossRef]
96. Wu, Y.L.; Wu, X. An optimized Forest-Ruth-like algorithm in extended phase space. *Int. J. Mod. Phys. C* **2018**, *29*, 1850006. [CrossRef]

97. Pan, G.F.; Wu, X.; Liang, E.W. Extended phase-space symplectic-like integrators for coherent post-Newtonian Euler-Lagrange equations. *Phys. Rev. D* **2021**, *104*, 044055. [CrossRef]
98. Luo, J.J.; Wu, X.; Huang, G.Q.; Liu, F.Y. Explicit symplectic-like integrators with midpoint permutations for spinning compact binaries. *Astrophys. J.* **2017**, *834*, 64. [CrossRef]
99. Wu, X.; Wang, Y.; Sun, W.; Liu, F.Y. Construction of Explicit Symplectic Integrators in General Relativity. IV. Kerr Black Holes. *Astrophys. J.* **2021**, *914*, 63. [CrossRef]
100. Zhou, N.; Zhang, H.; Liu, W.; Wu, X. Note on Construction of Explicit Symplectic Integrators for Schwarzschild Spacetimes. *Astrophys. J.* **2022**, *927*, 160. [CrossRef]
101. Mikkola, S. Practical symplectic methods with time transformation for the few-body problem. *Celest. Mech. Dyn. Ast.* **1997**, *67*, 145–165. [CrossRef]
102. Heydari-Fard, M.; Shirazi, M.; Jalalzadeh, S.; Sepangi, H.R. Accelarating universe in brane gravity with confining potential. *Phys. Lett. B* **2006**, *640*, 1–6. [CrossRef]
103. Heydari-Fard, M.; Razmi, H.; Sepangi, H.R. Brane-World Black Hole Solutions via a Confining Potential. *Phys. Rev. D* **2007**, *76*, 066002. [CrossRef]
104. Gurzadyan, V.G. On the common nature of dark matter and dark energy: Galaxy groups. *Eur. Phys. J. Plus.* **2019**, *134*, 14. [CrossRef]
105. Gurzadyan, V.G. Stepanian, A. The cosmological constant derived via galaxy groups and clusters. *Eur. Phys. J. C* **2019**, *79*, 169. [CrossRef]
106. Zwicky, F. On the large scale distribution of matter in the universe. *Phys. Rev.* **1942**, *61*, 489. [CrossRef]
107. Takamiya, T.; Sofue, Y. Radial distribution of the mass-to-luminosity ratio in spiral galaxies and massive dark cores. *Astrophys. J.* **2000**, *534*, 670. [CrossRef]
108. Honma, M.; Nagayama, T.; Ando, K. Bushimata, T. Fundamental parameters of the Milky Way galaxy based on VLBI astrometry. *Astron. Soc. Japan.* **2012**, *64*, 136.
109. Sofue, Y. Rotation Curve and Mass Distribution in the Galactic Center—From Black Hole to Entire Galaxy. *Astron. Soc. Japan* **2013**, *65*, 118. [CrossRef]
110. Shaymatova, S.; Malafarinaf, D.; Ahmedov, B. Effect of perfect fluid dark matter on particle motion around a static black hole immersed in an external magnetic field. *Phys. Dark Univ.* **2021**, *34*, 100891. [CrossRef]
111. Wu, P.; Yu, H. Observational constraints on f(T) theory. *Phys. Lett. B* **2010**, *693*, 415–420. [CrossRef]
112. Xie, Y.; Deng, X.M. f(T) gravity: Effects on astronomical observation and Solar system experiments and upper bounds. *Mon. Not. R. Astron. Soc.* **2013**, *433*, 3584. [CrossRef]
113. Deng, X.M. Probing f(T) gravity with gravitational time advancement. *Class. Quant. Grav.* **2018**, *35*, 175013. [CrossRef]
114. Deng, X.M. Geodesics and periodic orbits around quantum-corrected black holes. *Phys. Dark. Univ.* **2020**, *30*, 100629. [CrossRef]
115. Lin, H.Y.; Deng, X.M. Rational orbits around 4D Einstein-Lovelock black holes. *Phys. Dark. Univ.* **2021**, *31*, 100745. [CrossRef]
116. Liu, Y.C.; Feng, J.X.; Shu, F.W.; Wang, A.Z. Extended geometry of Gambini-Olmedo-Pullin polymer black hole and its quasinormal spectrum. *Phys. Rev. D* **2021**, *104*, 106001. [CrossRef]
117. Astier, P.; Pain, R. Observational evidence of the accelerated expansion of the universe. *Comptes Rendus Phys.* **2012**, 13, 521. [CrossRef]
118. Padmanabhan, T. Accelerated expansion of the universe driven by tachyonic matter. *Phys. Rev. D* **2002**, *66*, 021301. [CrossRef]
119. Schrabback, T.; Hartlap, J.; Joachimi, B.; Kilbinger, M.; Simon, P.; Benabed, K.; Brada, M.; Eifler, T.; Erben, T.; Fassnacht, C.D.; et al. Evidence of the accelerated expansion of the Universe from weak lensing tomography with COSMOS ⋆. *Astron. Astrophys.* **2010**, *516*, 63. [CrossRef]
120. Carter, B. Global Structure of the Kerr Family of Gravitational Fields. *Phys. Rev.* **1968**, *174*, 1559. [CrossRef]
121. Cao, W.; Liu, W.; Wu, X. Integrability of Kerr-Newman spacetime with cloud strings, quintessence and electromagnetic field. *Phys. Rev. D* **2022**, *105*, 124039. [CrossRef]